Chemical Physics Letters 651 (2016) 155–160

Contents lists available at ScienceDirect

Chemical Physics Letters

journal homepage: www.elsevier.com/locate/cplett

Magnetic proximity effect in ferrimagnetic–ferromagnetic core–shell Prussian blue analogues molecular magnet

Pramod Bhatt*, Amit Kumar, S.S. Meena, M.D. Mukadam, S.M. Yusuf*

Solid State Physics Division, Bhabha Atomic Research Centre, Mumbai 400 085, India

ARTICLE INFO

Article history:
Received 28 January 2016
In final form 19 March 2016
Available online 24 March 2016

ABSTRACT

A magnetic proximity effect has been observed in core–shell structure of molecular magnet, $Mn_{1.5}[Cr(CN)_6]\cdot mH_2O@Ni_{1.5}[Cr(CN)_6]\cdot nH_2O$, synthesized using a ferrimagnetic core of $Mn_{1.5}[Cr(CN)_6]\cdot 7.5H_2O$ surrounded by a ferromagnetic shell of $Ni_{1.5}[Cr(CN)_6]\cdot 7.5H_2O$. The values of Curie temperature (T_C) are found to be of ~65 and ~60 K for the bare–core and bare–shell compounds, respectively. However, an enhanced T_C (~70 K) has been observed for the core–shell structure. The proximity effect (due to presence of interface exchange coupling) between core and shell is responsible for the observed enhancement of T_C. A neutron depolarization study also confirms finite depolarization below ~70 K.

1. Introduction

The Prussian blue analogues (PBAs), with empirical formula $X_pA_q[B(CN)_6]_r\cdot zH_2O$ (A and B are transition metal ions, and X are alkali metal ions, as K^+ and Rb^+) have attracted many researchers because of their multifunctional properties [1]. Other properties of this class of compounds include magnetic pole inversion [2,3], photomagnetism [4,5], zero/negative thermal expansion [6], piezomagnetism [7]. Moreover, PBAs have possible wide technological applications [8] in magneto-optical switching [9], battery materials [10,11], hydrogen storage [12–14], ion exchange for the removal of Cs-137 [15,16], ion sensing [17,18], and electro- and photo-catalysis [19]. However, above mentioned multifunctional properties and their possible technological applications are not practically feasible in case of most of the PBAs as magnetic ordering temperatures are well below room temperature. Therefore, the synthesis of PBAs with a higher magnetic ordering temperature (Curie temperature, T_C) has always been a quest for many years. In order to increase the magnetic ordering temperature of PBAs, new approaches have been continuously implemented, such as synthesis of the PBAs by varying $3d/4f$ elements, introduction of alkali metal ions in the structure, varying reduction voltage and deposition time in electro-deposition methods and using various synthesis methods such as, co-precipitation, electrochemical, solution dip and dry, sequential adsorption technique, etc. In this regard, we have made few attempts earlier to enhance the T_C of PBAs [20–22].

The advance research has opened up new perspectives toward the design of new core–shell nanoparticles with new composition and fine control of their structure and magnetic properties [23,24]. The combination of two phases in a core–shell structure results in a magnetic interface at which exchange bias coupling generates an additional source of anisotropy [25]. Therefore, the synthesis of core–shell nanostructures, and investigation of their structural and magnetic properties for possible technological applications have been of current research interest.

The core–shell structures of PBAs [26–28] are known for interesting magnetic properties like charge-transfer induced spin transition switching [29] and persistent photo-induced magnetization [30]. The photo-switchable core with a $Rb_{0.2}Ni[Cr(CN)_6]_{0.7}\cdot zH_2O$ ferromagnetic shell has been reported for the charge-transfer induced spin transition switching properties, whereas $K_jNi_k[Cr(CN)_6]_l\cdot nH_2O$ as core with $Rb_aCo_b[Fe(CN)_6]_c\cdot mH_2O$ as shell has been synthesized for persistent photo-induced magnetization [30]. Moreover, other core–shell structures of PBAs were synthesized for the high redox stability, enhanced rate capability [31] and high capacity as a cathode material in batteries [32,33] and hydrogen storage applications [34]. We have earlier studied $Mn_{1.5}[Cr(CN)_6]\cdot mH_2O@Ni_{1.5}[Cr(CN)_6]\cdot nH_2O$ core–shell structure of PBAs for hydrogen storage applications [34]. However, in the present manuscript, we report magnetic properties investigation of the ferrimagnetic–ferromagnetic core–shell structure using powder neutron diffraction, *dc* magnetization, and temperature dependent neutron depolarization measurements. More interestingly, we report the enhancement

* Corresponding authors.
E-mail addresses: prabhatt@barc.gov.in (P. Bhatt), smyusuf@barc.gov.in (S.M. Yusuf).

http://dx.doi.org/10.1016/j.cplett.2016.03.047
0009-2614/

of T_C, arising due to magnetic proximity effect present in the ferrimagnetic–ferromagnetic core–shell structure of PBAs.

2. Experimental

The bare–core, bare–shell and core–shell samples are synthesized using the co-precipitation method. For the synthesis of the core–shell compound, we have followed the procedure previously described in the literature [29,30,32,34]. The 5 ml of the precipitated solution of the bare–core compound $Mn_{1.5}[Cr(CN)_6]\cdot 7.5H_2O$ is diluted in 20 ml of $K_3[Cr(CN)_6]$ solution. The particles are subsequently filtered before being washed with ultra-pure water, and re-dispersed in 100 mm of water for use in the next step. Then, the core–shell, $Mn_{1.5}[Cr(CN)_6]\cdot mH_2O@Ni_{1.5}[Cr(CN)_6]\cdot nH_2O$ structure is subsequently grown by simultaneous and drop wise addition (0.50 ml/min) of $Ni(II)(NO_3)_2\cdot 6H_2O$ (0.15 M, 10 ml) and $K_3[Cr(CN)_6]$ (0.1 M, 10 ml) solutions to the diluted core solution. The precipitate is filtered and washed many times with doubly distilled water and ethanol until the un-reacted materials (like K and Cl), have been removed from the compound.

The neuron powder diffraction measurements of all samples are performed over an angular (2θ) range of 10–50° using a five-linear-position-sensitive detector based neutron powder diffractometer-II ($\lambda = 1.24$ Å) at Dhruva reactor, Bhabha Atomic Research Centre (BARC), India. The geometry of the neutron diffraction experiments is presented in Supporting Figure S1a. A detailed structural analysis is performed on the neutron diffraction data by the Rietveld refinement method using the FULLPROF program [35]. The *dc* magnetization measurements are carried out using a Cryogenic Ltd., UK make, vibrating sample magnetometer as a function of both temperature and magnetic field. Magnetization as a function of magnetic field are recorded at ~5 K over +50 to −50 kOe applied magnetic field for all samples.

The polarization analysis spectrometer ($\lambda = 1.205$ Å) at Dhruva reactor, BARC, India is used for the neutron depolarization study. In this experiment, the sample is first cooled from room temperature to the lowest temperature of measurement (2 K) in the presence of 10 Oe field, and then the measurements are carried out in the warming cycle under the same field. The incident neutron beam is polarized along the $-Z$ direction (vertically down, because a $Cu_2MnAl(111)$ crystal, which has a negative polarization efficiency, was used as the polarizer) with a beam polarization of 98.60(1)%. The transmitted neutron beam polarization is measured along the $+Z$ direction (vertically up, because here a $Co_{0:92}Fe_{0:2}(200)$ crystal is used as the analyzer, which has a positive polarization efficiency). The detailed experimental process is described in an earlier paper [36]. All samples used for the present study are filled in a rectangular tube which is placed facing the neutron beam in such a way that the plane surface (XZ) of the sample is perpendicular to the propagation direction (Y) of the polarized neutron beam. The beam size is restricted to fall on the sample size with the help of a cadmium slit. The geometry of the neutron depolarization experiments is in Supporting Figure S1b.

3. Results and discussion

3.1. Neutron diffraction study

Figure 1 presents the Rietveld refined [37] room temperature neutron powder diffraction patterns of the bare–core, core–shell and bare–shell samples. The crystal structure of all the samples is *face centered cubic* (*fcc*) with the space group *Fm3m*. The refined neutron patterns of bare–core, and bare–shell samples confirm that, they are single crystalline. The lattice constants are found to be 10.68(5) and 10.42(8) Å for the bare–core, $Mn_{1.5}[Cr(CN)_6]\cdot 7.5H_2O$

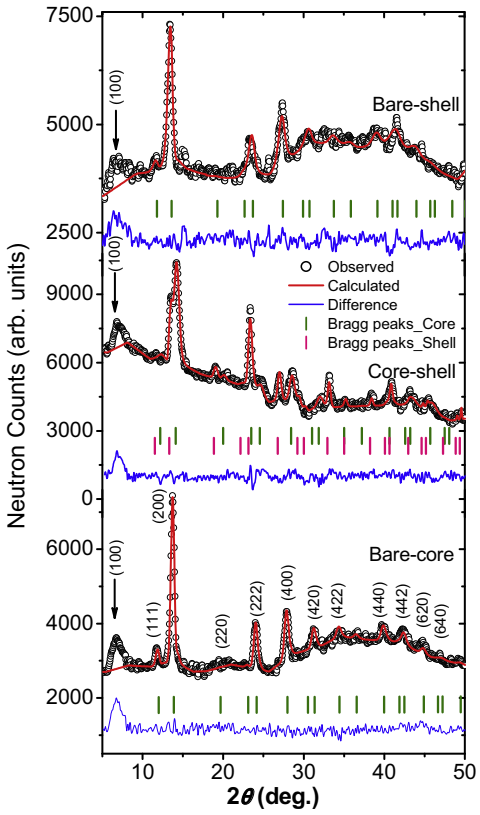

Figure 1. Rietveld refined room temperature neutron powder diffraction patterns of bare–core, bare–shell, and core–shell samples. Open circles and solid lines indicate the observed and the calculated patterns, respectively. Solid lines at the bottom show the difference between observed and calculated patterns. Vertical lines at the bottom of neutron diffraction patterns show the position of allowed Bragg peaks, and their corresponding (*hkl*) values are also marked for the bare–core sample. The Bragg peak (100), marked by an arrow for all samples, is due to structural disorder present in the samples.

and bare–shell, $Ni_{1.5}[Cr(CN)_6]\cdot 7.5H_2O$ samples, respectively. The lattice constant values of bare–core and bare–shell compounds are well in agreement with the previously reported [38] values of lattice constant of ~10.75 Å for $Mn_{1.5}[Cr(CN)_6]\cdot zH_2O$ and ~10.45 Å for $Ni_{1.5}[Cr(CN)_6]\cdot zH_2O$ compounds. The neutron diffraction pattern of the core–shell compound is found to fit best with the structural model comprising of both core and shell phases with the space group *Fm3m*. The weight fractions are found to be ~40 and 60% for the core and shell phases, respectively. The lattice constants for the core–shell structure, $Mn_{1.5}[Cr(CN)_6]\cdot mH_2O@Ni_{1.5}[Cr(CN)_6]\cdot nH_2O$ are found to be 10.35(8) and 10.70(3) Å, for the two phases, respectively. The important structural parameters, such as atomic coordinates and site occupancies, derived from the Rietveld analysis of neutron diffraction patterns of the bare–core, core–shell, and bare–shell are given in Table I as supporting information. The transition metal ions, Mn^{II} and Ni^{II} in the core–shell sample are located at the 4*a* (0, 0, 0) crystallographic position, while the Cr^{III} ions occupy the 4*b* (1/2, 1/2, 1/2) crystallographic position. The C and N reside at 24*e* (*x*, 0, 0) sites which are partially occupied due to $[Cr(CN)_6]$ vacancies. The number of total water molecules is estimated from the derived number of oxygen atoms, obtained from the fitted neutron patterns. The $[Cr(CN)_6]$ vacancies, and the coordinated and non-coordinated water molecules exhibit the structural disorder in the samples. The modulations in the background, and an extra Bragg peak (100), marked by an arrow in Figure 1 is the consequences of the structural disorder present in the compound.

The neutron powder diffraction pattern (Supporting Figure S2) of the core–shell sample, recorded at 6 K would result an